Measurements of Inelastic Energy Loss in Large-Angle Ar^+ on Ar Collisions at keV Energies*

GERRY H. MORGAN AND EDGAR EVERHART
Physics Department, University of Connecticut, Storrs, Connecticut
(Received June 8, 1962)

Large-angle collisions of Ar^+ ions with Ar atoms are studied in which the inelastic energy loss Q is measured as a function of incident energy and scattering angle. Measurements are made at 3-, 6-, 12-, 25-, 50-, 75-, and 100-keV incident energies and the recoiling target particles are studied at several angles ϕ between 84° and 52°, corresponding to collisions where the scattered incident particle is scattered through angles θ between about 6° and 38°. The kinetic energies and scattering angles of the recoils are accurately measured, and this, together with the conservation equations, permits determination of the inelastic energy. The average value of the inelastic energy loss $\bar{Q}$ is plotted vs recoil angle ϕ and a separate curve is obtained for each incident energy. However, when the various $\bar{Q}$ values are plotted vs the calculated distance of closest approach, a universal curve is obtained which has an abrupt rise when this distance is 0.23 Å irrespective of energy.

The $\bar{Q}$ values are a weighted average of the energy losses associated with the various charge states found among the recoil particles at a given angle, the energy loss $\bar{Q}_n$ of a particular charge state n being weighted in accordance with its abundance. The several values of $\bar{Q}_n$ are presented for each of several angles ϕ at each energy studied.

In a few cases a fine structure was seen in the data. For example, in 12-keV Ar^+ on Ar collisions, the recoils at $\phi=52°$ are found to contain Ar^{2+} ions (as well as Ar^+, Ar^{3+}, etc.). Here these Ar^{2+} ions arise from collisions where the average value is $\bar{Q}_2=234$ eV. However, this is a weighted average of three just resolved groups of slightly different energies and these correspond to Q's of 90, 318, and 620 eV. These are interpreted as arising from collisions where the (unobserved) scattered incident particle is Ar^+, Ar^{3+}, and Ar^{5+}, respectively. Thus, individual Q values are obtained for these reactions. There is evidence that the electrons usually leave in groups of two during these violent collisions.

1. INTRODUCTION

WHEN argon ions strike argon atoms at keV energies, some of the collisions result in large-angle scattering of both the incident particle and the recoil target particles. In these violent collisions it is found that the scattered particles may be highly ionized. It is the purpose of this work to measure the inelastic energy loss in these collisions for each state of ionization as a function of the scattering angle and the incident energy.

The combination Ar^+ on Ar was chosen for study because there are considerable supporting data available for this ion-atom combination. Thus, Fuls *et al.*[1] and Jones *et al.*[2] measured the differential cross section for scattering of Ar^+ on Ar at angles between 1° and 36° and at energies from 25 to 100 keV. Further data by Ziemba *et al.*[3] extended the range in energy from 10 to 140 keV at fixed 5° scattering angle. These data were used by Lane and Everhart[4] to determine the effect of electron screening on the effective potential energy function for Ar^+ on Ar collisions.

The scattered ions were analyzed[1–3] and all ionization states, ranging from Ar^0 to Ar^{7+}, are found in various proportions depending on the incident energy and the scattering angle. Russek and Thomas[5] have developed a theory which has been remarkably successful in predicting the above ionization proportions. However, the part of their theory wherein the inelastic energy loss is calculated as a function of scattering angle is not satisfactory, and the measurements of the present paper are needed.

Other measurements of large-angle Ar^+ on Ar collisions have been described by Fedorenko[6] and by Kaminker and Fedorenko.[7] Most important to the present work is the paper of Afrosimov and Fedorenko[8] who have measured inelastic energy loss in Ar^+ on Ar collisions at 75 keV for various scattering angles. Some of our data have been taken at 75 keV for the specific purpose of comparison with their data. It turns out that their data do not cover the same angular range as our data and thus provide an interesting extension to our results.

Besides the 75-keV energy mentioned above, our data were taken at six other energies: 100, 50, and 25 keV, since these are the energies for which the most extensive supporting data[1,2] were taken, and 12, 6, and 3 keV for a systematic extension to low energies.

Section 2 below describes the theory and shows how the inelastic energy may be obtained from accurate measurements of the angle and kinetic energy of the scattered recoil particle. Section 3 describes the apparatus and procedure in detail, and Sec. 4 presents the data. Here, the average inelastic energy is plotted vs scattering angle for each charge state at each energy.

* This work was sponsored by the U. S. Army Research Office, Durham.

[1] E. N. Fuls, P. R. Jones, F. P. Ziemba, and E. Everhart, Phys. Rev. **107**, 704 (1957), Figs. 9 and 15.

[2] P. R. Jones, F. P. Ziemba, H. A. Moses, and E. Everhart, Phys. Rev. **113**, 182 (1959), Fig. 7.

[3] F. P. Ziemba, G. J. Lockwood, G. H. Morgan, and E. Everhart, Phys. Rev. **118**, 1552 (1960), Fig. 9(a).

[4] G. H. Lane and E. Everhart, Phys. Rev. **120**, 2064 (1960).

[5] A. Russek and M. T. Thomas, Phys. Rev. **109**, 2015 (1958); **114**, 1538 (1959); J. B. Bulman and A. Russek, *ibid.* **122**, 506 (1961).

[6] N. V. Fedorenko, J. Tech. Phys. (U.S.S.R.) **24**, 784 (1954).

[7] D. M. Kaminkes and N. V. Fedorenko, J. Tech. Phys. (U.S.S.R.) **25**, 2239 (1955).

[8] V. V. Afrosimov and N. V. Fedorenko, J. Tech. Phys. (U.S.S.R.) **27**, 2557 (1957) [translation: Soviet Phys.—Tech. Phys. **2**, 2391 (1957)].

The data are discussed in Sec. 5 and compared with the results of the other workers mentioned above.

Section 6 describes a fine structure which is just resolved in some cases. This enables inelastic energy loss values to be given for reactions where both the recoil particle and the scattered incident particle are specified. This section also analyzes the evidence that electrons are removed two at a time during these violent collisions.

The Appendix discusses instrumental resolution problems.

2. THEORY OF THE MEASUREMENT

A. The Fundamental Equations

Let the incident particle, of mass m_1, and kinetic energy T_0, strike a stationary target particle of mass m_2. Let $\gamma=m_1/m_2$ be the ratio of these masses. After the collision the incident particle is deflected through an angle θ and has kinetic energy T_1, and the recoil target particle appears at angle ϕ with kinetic energy T_2. The inelastic energy loss is Q. The above angles and energies are measured in the laboratory frame of reference. Neglecting the momentum carried off by electrons, the conservation equations are

$$T_0=T_1+T_2+Q, \tag{1}$$

$$(\gamma T_0)^{1/2}=(\gamma T_1)^{1/2}\cos\theta+T_2^{1/2}\cos\phi, \tag{2}$$

and

$$0=(\gamma T_1)^{1/2}\sin\theta-T_1^{1/2}\sin\phi. \tag{3}$$

There are five measurable quantities T_0, T_1, T_2, θ, and ϕ, any three of which serve to determine Q with the above equations. However, if the quantities T_1 or θ pertaining to the scattered incident particle are measured simultaneously with T_2 or ϕ pertaining to the recoil particle, it is obviously necessary to use coincidence techniques to assure that particles from the same collision are being studied. To avoid this complication, it is desirable to measure either the set T_0, T_1, and θ, or the set T_0, T_2, and ϕ.

Of these two possibilities, it is much better to use the latter set wherein the energy and angle of the recoil particle are measured. The differential cross section is such that most of the scattered recoils will be found in the region $45°<\phi<90°$, where T_2 is considerably smaller than T_0, and most of the scattered incident particles will be found in the region $0°<\theta<45°$, where T_1 is more nearly comparable with T_0. It can be shown that T_2 is relatively sensitive to changes in Q in the angular region where most recoils are to be found, and that the opposite is true for T_1 in the angular region where most scattered incident particles are found.

It is useful to solve Eqs. (1)–(3) for $Q(T_0,T_2,\phi)$ and for $\theta(T_0,T_2,\phi)$, obtaining

$$Q=2T_2[(T_0/\gamma T_2)^{1/2}\cos\phi-(\gamma+1)/2\gamma], \tag{4}$$

and

$$\tan\theta=(\sin\phi)/[(\gamma T_0/T_2)^{1/2}-\cos\phi]. \tag{5}$$

B. Accuracy Requirements

In taking the data it is necessary to measure T_2/T_0 and ϕ with high accuracy because Q is small compared to any of the kinetic energies. The collision parameters differ but little from the values they would have if the collision were elastic and Q is found from the difference of two nearly equal terms in Eq. (4). As an illustrative example, consider the case of Ar^+ incident on Ar where $T_0=75$ keV and where the recoil particles at $\phi=52°$ are measured. Here the mass ratio γ is unity, and the recoil kinetic energy T_2 would be 28 419 eV if the collisions were elastic. However, the actually measured value of T_2 was 27 665 eV, and the value of Q, calculated using Eq. (4), was 749 eV. If this measured value of T_2 had been 0.3% higher, the calculated value of Q would have been 11% lower. Further numerical substitution in Eq. (4) shows that if the angle ϕ had been recorded as 52°00′ when it was actually 52°05′, this, in itself, would have caused a 14% error in Q. The accuracy requirements are not quite as severe when ϕ is larger. Thus, when $T_0=75$ keV and $\phi=78°$, an error of 0.3% in T_2 and 0°05′ in ϕ yield errors in Q of 1 and 5%, respectively. The necessary experimental precautions and calibrations are described in Sec. 3 below.

The effect of the finite resolution of the energy analyzer which measured T_2 and effects arising from the finite angular width in ϕ of the recoil particle detector is considered in detail in the Appendix. There it is shown that the average value of Q is properly calculated using Eq. (4), where T_2 is the center energy at which the analyzer is set and where the angle ϕ is that of the center line of the collimating slits of the detector.

C. Hard and Soft Components

In their work Afrosimov and Fedorenko[8] called attention to a most interesting feature of these collisions which must be discussed further here. Writing T_2 in terms of T_0, ϕ, and Q [equivalent to solving Eq. (4) for T_2], they obtain

$$T_2/T_0=[\gamma/(\gamma+1)^2]\{\cos\phi \pm[\cos^2\phi-(\gamma+1)Q/T_0]^{1/2}\}^2. \tag{6}$$

It is seen that there are two values of T_2 for each value of Q and ϕ. The recoil particles whose energy corresponds to the plus sign in Eq. (6) are called the "hard" component, and those corresponding to the minus sign are called the "soft" component.

There is a special condition which obtains when the square-root term in Eq. (6) equals zero. Although particles can appear at any angle ϕ less than 90°, to each angle ϕ there corresponds a maximum possible value of the energy loss, namely, $Q_{\max}(\phi)$, given by

$$Q_{\max}(\phi)=[T_0/(\gamma+1)]\cos^2\phi, \tag{7}$$

and for this particular value of Q the corresponding

recoil particle's energy is T_2' given by

$$T_2'=[T_0\gamma/(\gamma+1)^2]\cos^2\phi. \quad (8)$$

At this same angle ϕ the "hard" component of scattered particles will have a distribution in kinetic energies T_2 in excess of T_2' and the "soft" component will have a distribution in T_2 less than T_2'. For angles near 90°, the distribution in T_2 is wide and all values of Q up to $Q_{max}(\phi)$ are found, but for angles well removed from 90° the hard component will be found with values of T_2 distributed not far below the elastic energy and the soft component will be found very well separated with their energies T_2 of the order of one electron volt.

In our work, and in the previous work,[8] the soft component of recoil particles has been detected in some cases, but generally only the hard component is suitable for measurement of Q. Our apparatus was primarily designed to study recoil particles at angles well below 90°. This corresponds to studying the more violent collisions where the impact parameter is small and there is deep interpenetration of the atomic systems.

3. APPARATUS AND PROCEDURE

A. Outline of the Experiment

The Ar^+ ion beam was furnished by the University of Connecticut Cockcroft-Walton type accelerator. The ion beam is steered into the target gas chamber shown in Fig. 1 through small hole a which is 0.79-mm diam. A small Faraday cage m can be moved to intercept the ion beam and monitor its strength from time to time. Within the chamber there is argon gas at a pressure of about 1 μ, and most of the incident Ar^+ ions will transverse the chamber without making any collisions at all. About one in ten thousand of the Ar^+ ions will make a rare violent collision with an argon target atom in the vicinity of b, and of these only a few recoil particles will happen to be directed within the solid angle defined by holes c and d. These holes are both 0.59-mm diam and are located, in turn, 9.5 and 75.2 mm from point b. The conditions are such that the scattered particles result from single collisions.

The collimating holes c and d are aligned at angle ϕ with the incident ion beam and this angle is adjustable between 52° and 92°. A flexible metal bellows encloses part of the target gas chamber and allows this rotation about point b. The differential cross sections are such that (classically) practically all the particles which pass through slits c and d are recoiling target particles. Since they have suffered a violent collision, they are found in various states of ionization and with various kinetic energies. The scattered particles then pass between the plates of a cylindrical electrostatic analyzer, and those in each charge state (excluding neutrals) may be brought in succession through slit e where the particles are counted individually.

The interior of the apparatus is gold plated so that there will be no metal oxides on which static charges may settle and disturb the low-energy ion beams.

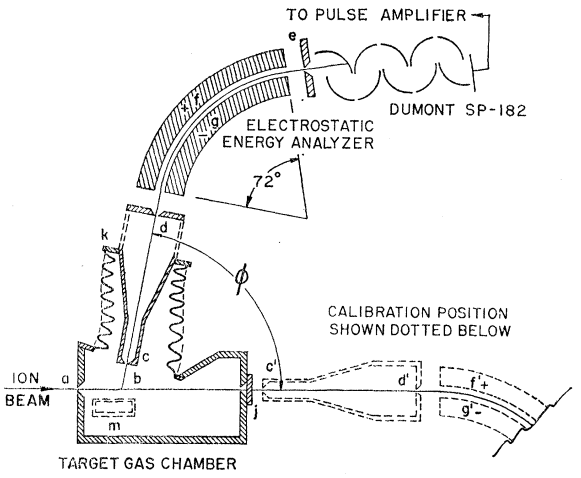

FIG. 1. The scattering apparatus.

B. Measurement of ϕ

As discussed in Sec. 2B, the angle ϕ must be very accurately determined. The graduated circle used in this measurement has, in itself, sufficient accuracy, but the difficulty lies in locating the 90° index mark at the point where the collimator slits are exactly perpendicular to the ion beam. This alignment was performed using an accurately machined mechanical jig. The estimated error in this process was 5′ arc. This measurement of ϕ is the source of the largest possible systematic error in the data.

C. Measurements of T_2

Obtaining the necessary accuracy in the ratio T_2/T_0 required several precautions. The electrostatic analyzer was designed to have desirable focusing properties[9] and its electrical center is at ground potential. From its known dimensions, it is easy to compute the relationship which should result between the analyzer voltage and the corresponding particle energy. However, it could not be used as an absolute measure because it was found experimentally that the indicated energy depended to some extent on the precise angle at which the ions enter the analyzer. A 1-deg change in this angle caused an intolerable 1.8% variation in apparent energy. To avoid this error, the structure holding collimating holes c and d was rigidly and permanently attached to the electrostatic analyzer. This assembly was calibrated by moving it bodily to the position shown dashed in Fig. 1. Then, with the obstruction at j removed, the incident ion beam entered through the collimator into the analyzer. The analyzer was then calibrated by comparison with the known incident beam energy. Thus, the ratio

[9] A. J. Dempster, Phys. Rev. 51, 67 (1937).

T_2/T_0 depends on measurements of T_2 and T_0 relative to the same standard and 0.07% estimate is made on the accuracy of this ratio.

The accelerator's high voltage and the analyzer voltage are both measured by precision wire-wound voltage dividers and readings are made with potentiometer circuits.

D. Procedure

With the accelerator energy T_0 set and the angle ϕ chosen, the electrostatic analyzer energy is set at a particular value. The scattered particles reaching the detector are now counted for a 5-sec interval. The incident ion beam is then intercepted for 5 sec and its value read on the monitor Faraday cage m. During this interception there are no recoil particles reaching the detector and the noise counts, if any, are recorded also. This counting procedure is repeated five times and averaged. The background noise is subtracted and the counting rate normalized to a fixed incident beam. This result is then plotted as a single point on one of the curves of Fig. 2(a,b) which plots the number of counts as a function of analyzer voltage for two typical cases. The procedure is repeated, taking 6 to 12 such points in tracing out the peaks for each of the several charge states shown in the figure. The "center of gravity" of each line is obtained by numerical integration.

The analyzer voltage plotted in Fig. 2(a,b) is scaled in accordance with the calibration so that it equals the kinetic energy of the singly ionized particles in electron volts. The energy of the doubly ionized peak is obtained by multiplying by two, and so on. The center energy T_2 for each charge state n and the angle ϕ are substituted into Eq. (4) to find the average value $\bar{Q}_n$ of inelastic energy for that charge state.

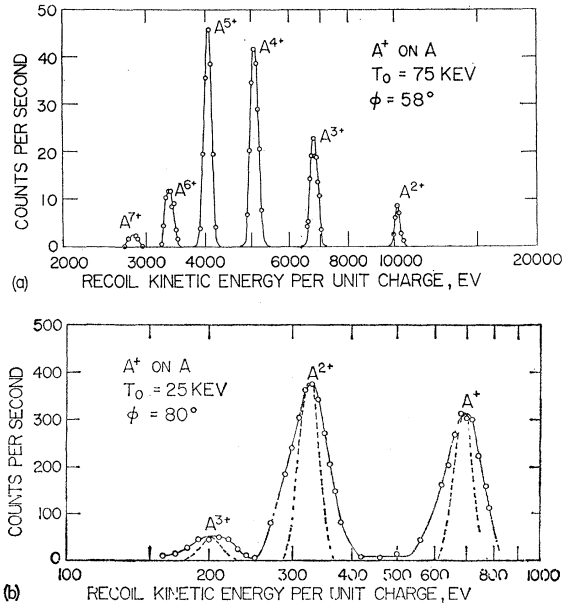

FIG. 2. (a) The kinetic energy per unit charge for the several charge components of recoil particles scattering at 58° from 75-keV Ar^+ on Ar collisions. The heights of the peaks are proportional to the relative abundances and their width is determined by instrumental resolution in this case. (b) As in (a), except for scattering at 80° from 25-keV Ar^+ on Ar collisions. The peaks here are wider than the instrumental resolution widths, which are shown dashed.

4. DATA

Figure 3 shows the data for Ar^+ on Ar collisions taken at 100-, 75-, and 50-keV energies, and Fig. 4 shows the data taken at 25-, 12-, 6-, and 3-keV energies. In each case the average inelastic energy loss $\bar{Q}_n$ for each charge state n is plotted vs the angle ϕ (in laboratory coordinates) at which the recoiling target particle is to be found. At the top of each graph is also shown the corresponding angle θ at which the scattered incident particle is to be found, calculated using Eq. (5).

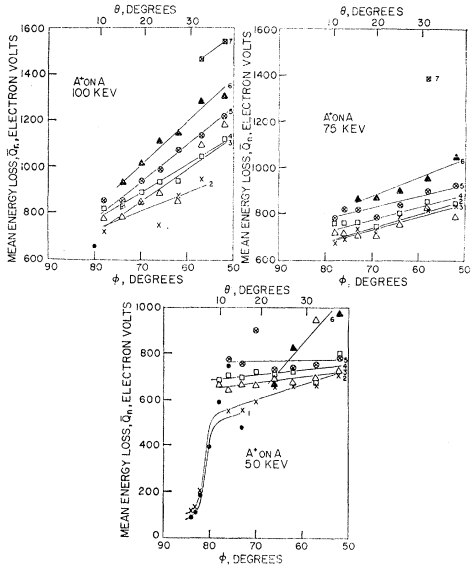

FIG. 3. The mean energy loss $\bar{Q}_n$ for each of the several charge states of recoil particles from Ar^+ on Ar collisions is plotted vs the recoil angle ϕ (laboratory coordinates). Indicated on the top edge are the corresponding angles θ for scattering of the incident particle. Data are presented for 100-, 75-, and 50-keV incident energies.

5. DISCUSSION

A. Average Inelastic Energy Loss

Figures 3 and 4 show that the higher charge states arise, as might be expected, from collisions where the average transferred energy is highest. For example, in the 100-keV case for scattering at the fixed angle of 52° it is evident that there must be a distribution in the $\bar{Q}_n$ values extending at least from 1100 to 1540 eV in this case. However, the data may be understood and discussed easily in terms of an average Q for each energy and angle.

The over-all average energy loss $\bar{Q}'$ is the weighted average of the average energy loss $\bar{Q}_n$ for each state. Thus,

$$\bar{Q}'=(\mathfrak{N}_1\bar{Q}_1+\mathfrak{N}_2\bar{Q}_2+\cdots)/(\mathfrak{N}_1+\mathfrak{N}_2+\cdots), \quad (9)$$

where $\mathfrak{N}_1$ is the number of singly ionized recoil particles counted, $\mathfrak{N}_2$ is the number of doubly ionized particles, etc. In our apparatus the neutral-recoil particles are not detected and their number and energy are unknown. The symbol $\bar{Q}'$ is used to distinguish the average energy without the neutrals from the average energy $\bar{Q}$ which would include the neutrals. The data of Fuls *et al.*[1] show that often there are very few neutrals, particularly for the more violent collisions at higher energies. Thus, $\bar{Q}'$ and $\bar{Q}$ are the same in many cases.

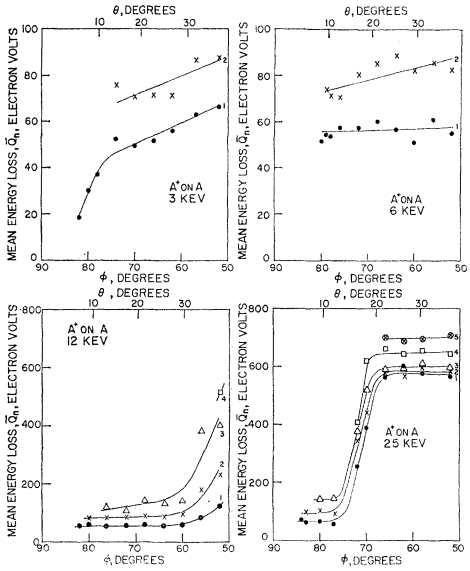

FIG. 4. The mean energy loss $\bar{Q}_n$ for each of the several charge states of recoil particles from Ar^+ on Ar collisions is plotted vs recoil angle ϕ, (laboratory coordinates). Indicated on the top edge are the corresponding angles θ for scattering of the incident particle. Data are presented at 3, 6, 12, and 25 keV.

Figure 5 shows a summary of the data wherein the average $\bar{Q}'$ is plotted vs the corresponding angle ϕ of the scattered incident particle. The most salient feature is the sharp increase in $\bar{Q}'$ which occurs to the extreme right of the 12-keV curve, in the center of the 25-keV curve, and on the left of the 50-keV curve.

B. Comparison with Other Data

The 75-keV data of Afrosimov and Fedorenko[8] are also plotted on Fig. 5 and they show a rapid increase in $\bar{Q}'$ consistent with our curves. However, there does appear to be a scale factor discrepancy between our data and theirs. The apparatus of Afrosimov and Fedorenko[8] uses a mass spectrometer in place of the electrostatic analyzer of Fig. 1 and it turns out that their apparatus is

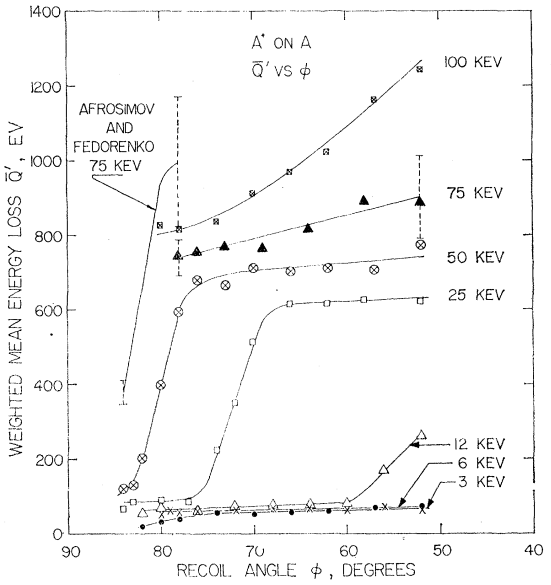

FIG. 5. The weighted mean energy loss is $\bar{Q}'$ plotted vs the recoil angle ϕ for Ar^+ on Ar collisions at 3-, 6-, 12-, 25-, 50-, 75-, and 100-keV incident energies. The 75-keV data of Afrosimov and Fedorenko are also shown.

better adapted to taking data with ϕ near 90°, corresponding to small values of θ. On the other hand, our apparatus is better adapted for taking data where ϕ is not too near 90°, corresponding to larger values of θ and more violent collisions.

The sharp increase in the $\bar{Q}'$ values for the 25-keV case is correlated with data taken by Fuls *et al.*[1] at the same energy. Figure 6(a) shows his data for ionization probabilities P_n plotted vs incident scattering angle θ and this shows a pronounced activity at 16° where the average degree of ionization increases sharply. Plotted below as the solid line in Fig. 6(b) are our 25-keV data of $\bar{Q}'$ vs θ which show a sudden rise at the same angle.

C. Comparison with the Russek-Thomas Theory

Russek and Thomas[5] have developed a theory whose connection with our work may be described with reference to Fig. 6. Their purpose was to predict the ionization probabilities P_n. They assume that when two argon atoms collide, the inelastic energy available to each atom is statistically distributed among the eight outer electrons and this enables a certain number of electrons to "boil off" leaving the collision products ionized. Their theory was remarkably successful in that the "peak heights" and "intersection heights" of the various ionization probabilities as in Fig. 6(a) were correctly predicted, and this part of the theory is quite independent of the relationship between the inelastic energy and the scattering angle. However, their values of P_n were plotted vs an arbitrary multiple of Q and the data of Fuls *et al.*[1] were plotted vs θ. In the absence of a satisfactory theory relating Q to θ, Russek and Thomas ob-

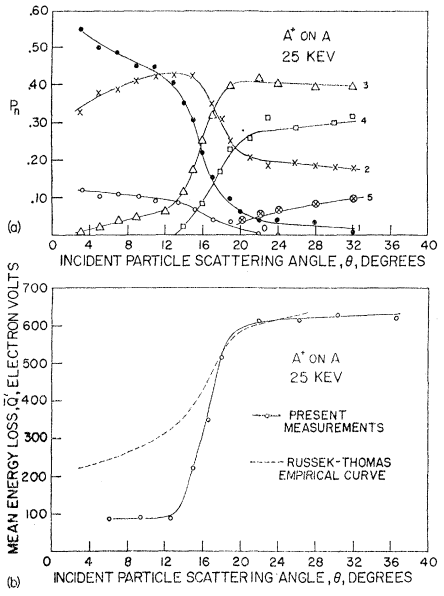

FIG. 6.(a) The charge-state probabilities P_n of the scattered incident particles are plotted vs its scattering angle θ for 25-keV Ar^+ on Ar collisions. The numbers 0, 1, ···, 5 identify the charge states n. These data, from the paper by Fuls *et al.*, show rapid changes in average ionization at about 16°. (b) The mean energy loss $\bar{Q}'$ is plotted vs θ for case (a). This shows a rapid rise at about 16° consistent with the data of (a). Also shown dashed is a semi-empirical curve by Russek and Thomas which is here adjusted to fit the data at large values of θ.

tained an empirical relation between these quantities (the dotted curve on the left of Fig. 10 in the first Russek-Thomas[5] paper) and this is shown dashed on our Fig. 6(b) for comparison with our measurements.

The Russek-Thomas empirical curve included an unknown "average ionization energy," and we have chosen this so that their dotted curve fits our measured curve at large values of θ. The solid measured curve and the dashed curve have similar shapes and inflect at the same place, but the dashed curve seems to require one scale factor adjustment at small angles and a different scale factor adjustment at large angles. Taking into account that the inelastic energy is shared by two atoms, and noting that the energy scale of the Russek-Thomas curves is plotted vs ϵ (where ϵ is one-fourth the average ionization energy), it is found that to fit our data curve at large angles θ requires an average ionization energy of 50 eV per electron; whereas to fit our data at small angles θ requires an average ionization energy of 16 eV per electron. In a recent paper Russek[10] suggests that the average ionization energy per electron may increase with the severity of the collision, and this is consistent with our results above.

D. Evidence for a Critical Interatomic Distance

It is interesting to plot $\bar{Q}'$ vs r_0, the distance of closest actual approach between the two atomic centers during the collision. (Here, r_0 is, of course, somewhat greater than the impact parameter.) The necessary relationships between r_0 and θ at various energies for Ar^+ on Ar collisions is readily obtained using tabulated calculations by Everhart *et al.*,[11] which are based on an appropriate screened Coulomb potential-energy function. There is good experimental evidence[1,4] that this function describes the trajectories of the scattering centers during the collision very well because it correctly predicts the measured differential cross sections.

The result is shown in Fig. 7 which plots $\bar{Q}'$ in electron volts as a function of r_0 in Angstrom units for various incident energies. Also indicated along the top of the figure are the approximate radii of the K and L shells of an argon atom and this provides a scale of the atomic size. It is significant that the rapid increase in $\bar{Q}'$ occurs when the interatomic least distance is 0.23 Å for all incident energies. A further abrupt rise is seen where this distance is 0.09 Å. The fact that the Q values depend more on interatomic distance than on incident energy in Ar^+ on Ar collisions recalls early work by Carbone *et al.*[12] and by Fedorenko[6] who observed that the ionization probabilities behaved in the same way.

E. Inelastic Energy vs Electron Loss

Over the range of collision parameters covered by the present data it is possible to obtain a universal relationship between the average inelastic energy and the average number $\bar{n}$ of electrons removed from both

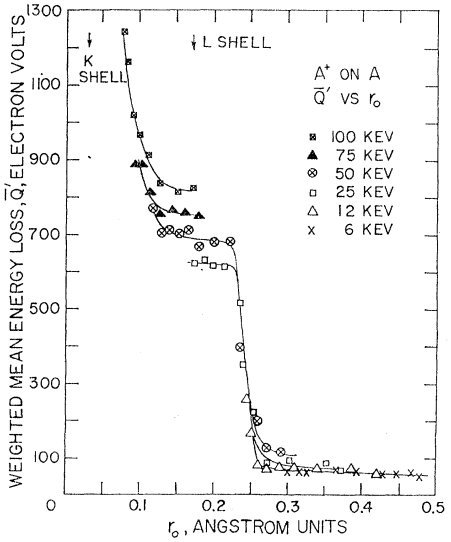

FIG. 7. The mean energy loss $\bar{Q}'$ is plotted vs the calculated distance of closest approach in large angle Ar^+ on Ar collisions. The curve includes data taken at six different energies and is largely independent of energy. There is a rapid rise at 0.23 Å and again at 0.09 Å. The radii of the K and L shells of a single argon atom are indicated at the top edge for comparison.

[10] A. Russek, Trans. N. Y. Acad. Sci. **23**, 681 (1961), see p. 688.

[11] E. Everhart, G. Stone, and R. J. Carbon, Phys. Rev. **99**, 1287 (1955).

[12] R. J. Carbone, E. N. Fuls, and E. Everhart, Phys. Rev. **102**, 1524 (1956).

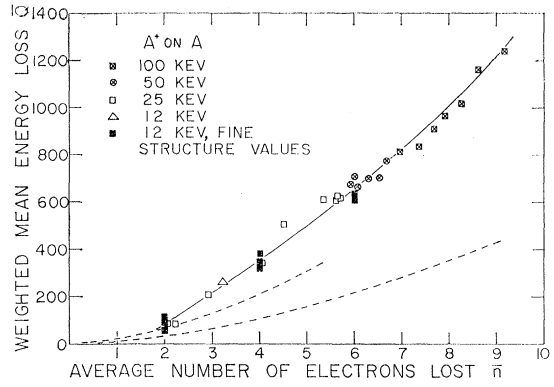

FIG. 8. The mean energy loss $\bar{Q}$ is plotted vs the average total number $\bar{n}$ of electrons lost from both atoms in violent Ar^+ on Ar collisions. This universal curve includes data taken at 12, 25, 50, and 100 keV. The solid points at $\bar{n}=2$, 4, and 6 electrons are obtained by an analysis of the fine structure seen in 12-keV data at $\phi=52°$. The dashed lines bound the values calculated from the ionization potentials without allowing for excess electron kinetic energies, excitation, or photon emission.

argon atoms during the collision. Here $\bar{n}$ may be calculated using $\bar{n}=\bar{n}_s+\bar{n}_r-1$, where $\bar{n}_s$ is the average number of electrons missing from the scattered incident particle, $\bar{n}_r$ is the average number of electrons missing from the recoil, and unity is subtracted to allow for the net deficiency of one electron before the collision.

The average value $\bar{n}_s$ is easily calculated from data giving the relative proportions P_n of the various charge states among the scattered incident particle. The necessary data, at various scattering angles θ, are given for energies of 25, 50, and 100 keV by the Ar^+ on Ar curves of Fuls *et al.*[1] [See also Fig. 6(a) of the present paper.] Thus, $\bar{n}_s=\sum nP_n/\sum P_n$. In a similar manner the corresponding average $\bar{n}_s$ for the recoils is calculated using data as in Fig. 2(a,b) wherein the peak heights give the relative proportions of the several charge states. Although the neutrals were not detected and were not allowed for in the calculation of $\bar{n}_r$, they are estimated to be few in number at these energies and angles and so the correction would be small.

The value of $\bar{Q}'$, which also neglects the neutrals, was first calculated as described in Sec. (5a) above. An approproximate calculation of $\bar{Q}$ was then carried out allowing for the effects of the neutrals. Here, it was assumed that the proportion of neutrals was the same for the recoils at angle ϕ as for the scattered incident particles at the corresponding angle θ, and that the value of $\bar{Q}_0$ was halfway between zero and the value of $\bar{Q}_1$. The values of $\bar{Q}$ so obtained differed hardly at all from the values of $\bar{Q}'$ obtained earlier.

The result of these calculations is given in Fig. 8 which plots $\bar{Q}$ vs $\bar{n}$. This incorporates the 25-, 50-, and 100-keV data calculated as described above and some 12-keV data calculated from the present results alone. Three sets of solid points at $\bar{n}=2$, 4, and 6 are also included as obtained from the fine structure measurements described in Sec. 6.

For comparison, there is also shown in Fig. 8 a pair of dashed curves which bound the possible net changes in total spectroscopic ionization energy. For example, in the particular reaction $Ar^+ + Ar \rightarrow Ar^{3+} + Ar^{2+} + 4e^-$ the difference in ionization energy before and after the collision is 111.85 eV. Another possible reaction where 4 electrons are lost is that in which the products are Ar^+ and Ar^{4+} for which the before-after difference is 145.19 eV. Still another $n=4$ reaction, with products Ar^0 and Ar^{5+}, yields a difference of 207.51 eV. The upper dashed line is drawn through the highest net ionization energy differences at each value of n and the lower dashed line is drawn through the lowest net ionization energy difference. This lower line invariably corresponds to cases where the two collision products are equally, or nearly equally, ionized and is expected to be much more representive of typical cases than the upper line. The difference in energy between the lower dashed curve and the measured $\bar{Q}$ values must be accounted for by the excess kinetic energy of the electrons and by photon emission from excited states.

Hasted[13] has made a study of the Ne^+ on Ar case in which the above possibilities are considered. Using data of Afrosimov and Fedorenko[8] and of Fuls *et al.*,[1] and the Russek-Thomas[5] theory, he finds evidence for electron kinetic energies totaling hundreds of electron volts.

6. FINE STRUCTURE

The separate peaks traced out by the energy distribution of each component of the recoils usually show a simple structure as in Fig. 2(a,b), but a just-resolved fine structure was seen in some cases. The data taken at 12 keV for $\phi=52°$ are presented in Fig. 9, which shows

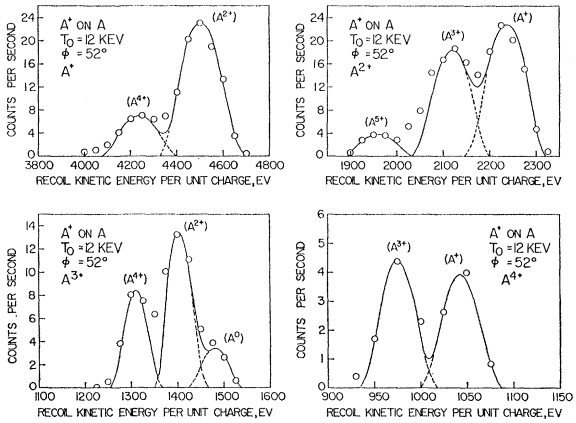

FIG. 9. The four separate figures show, respectively, the fine structure in kinetic energy for Ar^+, Ar^{2+}, Ar^{3+}, and Ar^{4+} recoils from 12-keV Ar^+ on Ar collisions at $\phi=52°$. Each of the resolved lines is thought to correspond to a particular charge state (as marked in parentheses) for the unobserved scattered incident particle. In every case there is a net loss of 2, 4, or 6 electrons. The instrumental resolution line shape is indicated.

[13] J. B. Hasted, Proc. Phys. Soc. (London) **77**, 269 (1961).

TABLE I. The Q values for each of the resolved recoil peaks at 12 keV and $\phi=52°$.

Recoil	Q values (eV)			$\bar{Q}_n$ (eV)
Ar^+	60	319		125
Ar^{2+}	90	318	620	234
Ar^{3+}	119	344	610	402
Ar^{4+}		383	634	515

two or three discrete kinetic energies for each of the charge states.

A. Identification

It is believed that each of the discrete peaks arises from a collision where the unobserved scattered incident particle had a particular charge state. Thus, for example, the three peaks for the Ar^{2+} recoils are thought to arise from collisions where the scattered incident particle must have been Ar^+, Ar^{3+}, and Ar^{5+}, respectively, as marked for this case in Fig. 9. The problem is first to see whether this identification is consistent with the Q values.

Table I gives the Q values for each of the resolved peaks of Fig. 9 grouped in three columns according to their approximate magnitudes.

Referring now to Fig. 8, it is seen that the Q's in the three columns of Table I correspond to the net loss by the two atoms of 2, 4, and 6 electrons, respectively. Thus the middle peak for the Ar^{2+} recoils corresponds to 4 electrons lost and the scattered incident particle must have been Ar^{3+} for that peak. In the same way all the peaks in Fig. 9 are identified and marked.

The next step is to see whether this identification is consistent with the expected relative abundances. Table II tabulates the heights of each of the peaks and is arranged so that the sum of the horizontal rows gives the abundance of the recoil particles charge states, and the sum of the vertical columns gives the abundance of the scattered incident particle charge states.

Disregarding the neutrals and the Ar^{5+}, which were not looked for among the recoils, the two abundances are in the same general proportions as would be expected for this symmetrical Ar^+ on Ar collision. This lends additional support to the assigned identification as marked on Fig. 9. Other identification patterns were tried also, corresponding to various numbers of electrons lost for each of the columns of Table I. These patterns included 0, 1, 2; 1, 2, 3; 1, 3, 5; 2, 3, 4; and 0, 2, 4 electrons lost for these columns, respectively. Not only are these other patterns not consistent with the data of Fig. 8, but they also do not give reasonable abundances in a compilation such as that of Table II.

It is not known from these data whether the electrons *always* leave in groups of two, or whether they *usually* do. The data are at the limit of resolution of the apparatus and there may be weak peaks in between the resolved peaks of Fig. 9.

TABLE II. Relative abundances in arbitrary units of recoil particle and scattered incident particle charge states for 12-keV Ar^+ on Ar scattering when $\phi=52°$.

Recoil particle	Scattered incident particle abundance						Recoil relative abundance
	Ar^0	Ar^+	Ar^{2+}	Ar^{3+}	Ar^{4+}	Ar^{5+}	
Ar^+			23		7		30 (Ar^+)
Ar^{2+}		23		18		4	45 (Ar^{2+})
Ar^{3+}	4		14		8		26 (Ar^{3+})
Ar^{4+}		4		4			8 (Ar^{4+})
Total	4	27	37	22	15	4	

B. Q's for Particular Reactions

Having identified the charge states of both the recoil particle and the scattered incident particle, the Q's for a number of Ar^+ on Ar reactions are known at 12 keV and $\phi=52°$. A reaction such as $Ar^+ + Ar \rightarrow Ar^{3+} + Ar^{2+} + 4e^-$, where Ar^{3+} is the scattered incident particle and Ar^{2+} is the recoil, is identified by the code 10/32 where the numbers refer, respectively, to the charge state of the incident particle, the target, the scattered incident particle, and the recoil. Table III gives Q's for the reactions which have been measured, and these are grouped, where possible, in pairs in which the scattered incident particle and the recoils are interchanged. It might be expected that these pairs should have the same Q, and, indeed, it is possible that the differences seen are the result of experimental error. However, it is interesting to note that for each pair the Q is higher in the reaction where the recoil has the higher charge state. Assuming that this effect is real, one can suggest a possible explanation: The momentum carried off by the electrons has been ignored in Eqs. (1)–(4). There may be an asymmetry along the line joining the atom centers such that more electrons are directed one way than the other as the departing particles become differently ionized. Not taking this into account may make an apparent difference in Q.

TABLE III. The Q's for particular Ar^+ on Ar reactions at 12 keV and $\phi=52°$.

Reaction	Q (eV)	Reaction	Q (eV)
10/21	60	10/43	610
10/12	90	10/34	634
10/32	318	10/52	620
10/23	344		
10/41	319	10/03	119
10/14	383		

C. Resolution Conditions

Only the 12-keV data at $\phi=52°$ and 56° showed fine structure fairly well resolved. Although the instrumental

resolution is best when ϕ is well removed from 90° (as discussed in the Appendix), this is not a sufficient condition because the fine structure was not resolved at other energies at these values of ϕ. It is also necessary that $\Delta Q/T_2$ be as large as possible. Here, ΔQ is the difference between the successive $\bar{Q}_n$ values. The 12-keV data in Fig. 4 show wide separation in the $\phi=52°$ data and ΔQ is large here. It is probably significant that the rapid change in Q values seen in the several curves of Figs. 3, 4, 5, and 7 also corresponds to wide separation of the $\bar{Q}_n$ values and happens to occur at an angle, in the 12-keV case, where the instrumental resolution is best. One might also expect to see fine structure at 25 keV for $\phi=72°$ and at 100 keV at $\phi=52°$. In fact, in these latter two cases, as well as in a few others, the lines do show structure, which is, however, not resolved quite well enough for detailed analysis.

ACKNOWLEDGMENTS

The authors wish to thank David E. Flinchbaugh who helped to operate the accelerator and who made a number of useful suggestions. Professor Arnold Russek has been most interested in these measurements and has contributed valuable discussions. The generosity of the University of Connecticut Computing Center is appreciated for making available their digital computer, for which the funds were contributed by the National Science Foundation.

APPENDIX

A. Effects of Finite Resolution

The effects of the finite angular resolution of the recoil collimator and the finite energy resolution of the cylindrical energy analyzer are several: (1) An apparent distribution in energy is recorded when none may exist. (2) A naturally existing distribution in energy is broadened and, consequently, the ability of the apparatus to resolve fine structure is limited. (3) The apparent mean energy of a distribution may be shifted from its true value.

B. The Analysis

The finite width of the peaks in Figs. 2 and 9 is largely due to finite instrumental resolution and this effect may be estimated and understood by assuming that the natural linewidths are ideally narrow and calculating the expected line shapes taking into account the apparatus. Thus, it is assumed that a particular charge component arises from a collision where the Q value is substantially constant over a small angular range in ϕ near the angle ϕ_0 at which the analyzer is set.

At the scattering point b of Fig. 1 the recoil particles will originate as $\sigma_r(\phi)d\phi$ where $\sigma_r(\phi)$ is the differential scattering cross section of the recoil particle in the laboratory frame. The passage of recoil particles through holes c and d is modified by a geometrical transmission factor $A(\phi_0,\phi)$ which is unity at $\phi=\phi_0$ and drops to zero when $|\phi_0-\phi|$ reaches 0.5°, the numerical value of the extreme acceptance width in the present apparatus. Thus, recoil particles which have passed through the collimator holes thus have a distribution $N_1(\phi)$ given by

$$N_1(\phi)d\phi=\sigma_r(\phi)A(\phi_0,\phi)d\phi. \tag{10}$$

Although Q is constant, the distribution $N_1(\phi)$ in angle is equivalent to a distribution $N_2(T_2)$ in the recoil kinetic energy T_2. The transformation $\phi=\phi(T_2)$ is given in Eqs. (4) or (6). The distribution of particles about to enter the energy analyzer is thus

$$N_2(T_2)dT_2=\sigma_r(\phi(T_2))A(\phi_0,\phi(T_2))(d\phi/dT_2)dT_2 \tag{11}$$

The midpoint energy to which the analyzer is set is T_{2m} but it passes particles according to a "window" $G(T_{2m},T_2)$ which is unity at $T_2=T_{2m}$, is fairly flat over a small range in T_2, and then drops rapidly to zero when T_2 differs from T_{2m} by 2% (in our case). The distribution $N_3(T_{2m})$ in particles passing through the electrostatic analyzer is found by integrating over the window width in T_2. Thus,

$$N_3(T_{2m})=\int_{T_2} G(T_{2m},T_2)N_2(T_2)dT_2 \tag{12}$$

is the formal expression for this distribution.

Numerical calculations were carried out in a number of cases. It turns out that the resolution is best when ϕ is well removed from 90°, being five times as narrow at $\phi=52°$ as it is at $\phi=83°$. The width of the lines in Fig. 2(a) is almost entirely due to instrumental resolution effects. In the cases illustrated in Fig. 9 the calculated instrumental resolution curve is drawn under each of the just-resolved components. In the case of Fig. 2(b) the instrumental resolution, shown dashed, is considerably more narrow than the measured profiles. In this case, where ϕ is near 90°, there is a suggestion that a fairly broad natural distribution exists in the Q values.

C. Instrumental Effects on Q Values

In Sec. 2(b) above it was noted that the center angle ϕ_0 must be measured to within a few minutes of arc and the analyzer energy T_{2m} to within accuracies of tenths of a percent. Since the actual collimator accepted particles over a range of ±0.5° in the angle, and since the analyzer had a window width of ±2% in energy, it was important to be sure that these instrumental effects, together with the asymmetrical $\sigma_r(\phi)$ function in Eq. (10) do not cause an appreciable shift in the apparent value of Q.

The procedure was to choose a value of Q equal to the measured value and calculate the ideal distribution $N_3(T_{2m})$ as in Eq. (12). From this, the central value of

T_2 was used to calculate again the value of Q using Eq. (4). In general, this new value of Q differs slightly from the original value because the asymmetry of the $\sigma_r(\phi)$ function contributes more particles from one side of the angular acceptance range than from the other side. The apparent shift in Q values from this cause was calculated for a number of cases and found to be largest where ϕ is near 90°. However, in the particular angular range of our measurements, this error in Q was found to be less than 1%.

PHYSICAL REVIEW VOLUME 128, NUMBER 2 OCTOBER 15, 1962

Second-Order Effects of Nuclear Magnetic Fields*

MORTON M. STERNHEIM
Brookhaven National Laboratory, Upton, New York
(Received June 14, 1962)

Using the Dirac equation, we consider the contributions to atomic levels of terms quadratic in **A**. **A** may be, for example, the nuclear magnetic dipole field. We show that a consistent quantum mechanical treatment cancels all terms arising from $[A_i,A_j]\neq 0$. This resolves a disagreement between hyperfine structure corrections calculated nonrelativistically and relativistically.

IN this note we consider the contributions to atomic levels of terms which are quadratic in **A**, where **A** is, for example, a nuclear magnetic dipole field. We will see that if A_i and A_j do not commute, a correct quantum mechanical treatment nevertheless cancels all terms arising from this noncommutativity. This result explains the disagreement between various hyperfine structure (hfs) calculations.

Consider an electron moving in the field of a fixed nucleus. Its motion is given by the Dirac equation,

$$[\beta m+\boldsymbol{\alpha}\cdot(\mathbf{p}+e\mathbf{A})-e\phi]\psi=E\psi, \tag{1}$$

where ϕ is the nuclear Coulomb potential. Treating

$$V\equiv e\boldsymbol{\alpha}\cdot\mathbf{A}$$

as a perturbation, for a state i we obtain to order A^2

$$\Delta E_i=\langle i|V|i\rangle+\sum_{n=+,-}{}'\langle i|V|n\rangle\langle n|V|i\rangle(E_0-E_n)^{-1}, \tag{2}$$

where n is summed over all positive and negative energy Coulomb states but i.

If i is a positive energy state, the Pauli approximation gives

$$\Delta E_i=\langle i|V_+|i\rangle+\sum_{n=+}{}'\langle i|V_+|n\rangle\langle n|V_+|i\rangle(E_0-E_n)^{-1}+\sum_{n=-}\langle i|V|n\rangle\langle n|V|i\rangle(E_0-E_n)^{-1}, \tag{3}$$

where

$$V_+=(e/m)\mathbf{p}\cdot\mathbf{A}+(e/2m)\boldsymbol{\sigma}\cdot\mathbf{H}. \tag{4}$$

In the negative-energy sum we can replace (E_0-E_n) by $2m$ and then sum over all states, including the positive-energy levels. Thus, this term becomes $(e^2/2m)\langle i|V^2|i\rangle$, and

$$\Delta E_i=\langle i|V_+|i\rangle+\sum_{n=+}{}'\langle i|V_+|n\rangle\langle n|V_+|i\rangle(E_0-E_n)^{-1}+(e^2/2m)\langle i|A^2+i\boldsymbol{\sigma}\cdot\mathbf{A}\times\mathbf{A}|i\rangle. \tag{5}$$

All the terms in Eq. (5) are familiar from the usual Foldy-Wouthuysen[1] and Pauli[2] reductions except for the one proportional to $\boldsymbol{\sigma}\cdot\mathbf{A}\times\mathbf{A}\equiv\sigma_iA_jA_k\epsilon_{ijk}$. This vanishes if **A** is a *classical* field, i.e., if A_j and A_k commute. However, if **A** contains the nuclear spin operator, then

$$[A_j,A_k]\neq 0. \tag{6}$$

The point that we wish to make is that if (6) holds, **A** is not a classical field despite the static nature of the source. A proper quantum mechanical treatment, in terms of Feynman graphs or old-fashioned noncovariant quantum electrodynamics, does not lead to Eq. (5).

Figure 1 shows the two Feynman graphs quadratic in **A**. With k, k', $p\sim Z\alpha m$, the crossed diagram is smaller by $Z\alpha$ than the uncrossed diagram for positive energy states. However, for negative energy states these diagrams differ to lowest order only in the ordering of

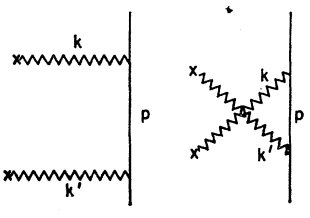

FIG. 1. The Feynman graphs quadratic in A.

* Work performed under the auspices of the U. S. Atomic Energy Commission.

[1] L. L. Foldy and S. A. Wouthuysen, Phys. Rev. 78, 29 (1950).
[2] H. A. Bethe and E. E. Salpeter, *Encyclopedia of Physics*, edited by S. Flügge (Springer-Verlag, Berlin, 1957), Vol. XXXV, p. 140.